Mon. Not. R. Astron. Soc. **000**, 1–12 (2016) Printed 28 November 2016 (MN LaTeX style file v2.2)

A search for long-timescale, low-frequency radio transients

Tara Murphy[1,2⋆], David L. Kaplan[3], Steve Croft[4,5], Christene Lynch[1,2], J. R. Callingham[1,6,2], Keith Bannister[6], Martin E. Bell[6,2], Natasha Hurley-Walker[7], Paul Hancock[7,2], Jack Line[8], Antonia Rowlinson[9,10], Emil Lenc[1,2], H. T. Intema[11,12], P. Jagannathan[11,13], Ronald D. Ekers[6,7], Steven Tingay[7,14], Fang Yuan[15,2], Christian Wolf[15,2], Christopher A. Onken[15,2], K. S. Dwarakanath[16], B.-Q. For[17], B. M. Gaensler[1,18,2], L. Hindson[19], M. Johnston-Hollitt[19], A. D. Kapińska[17,2], B. McKinley[8,2], J. Morgan[2], A. R. Offringa[9], P. Procopio[8,2], L. Staveley-Smith[17,2], R. Wayth[7], C. Wu[7], Q. Zheng[19]

[1] *Sydney Institute for Astronomy, School of Physics, The University of Sydney, NSW 2006, Australia*
[2] *ARC Centre of Excellence for All-sky Astrophysics (CAASTRO)*
[3] *Department of Physics, University of Wisconsin–Milwaukee, Milwaukee, WI 53201, USA*
[4] *Astronomy Department, University of California, Berkeley, 501 Campbell Hall #3411, Berkeley, CA 94720, USA*
[5] *Eureka Scientific, Inc., 2452 Delmer Street Suite 100, Oakland, CA 94602, USA*
[6] *CSIRO Astronomy and Space Science (CASS), Marsfield, NSW 2122, Australia*
[7] *International Centre for Radio Astronomy Research, Curtin University, Bentley, WA 6102, Australia*
[8] *School of Physics, The University of Melbourne, Parkville, VIC 3010, Australia*
[9] *Netherlands Institute for Radio Astronomy (ASTRON), PO Box 2, 7990 AA Dwingeloo, The Netherlands*
[10] *Anton Pannekoek Institute, University of Amsterdam, Postbus 94249, 1090 GE, Amsterdam, The Netherlands*
[11] *National Radio Astronomy Observatory, 1003 Lopezville Road, Socorro, NM 87801-0387, USA*
[12] *Leiden Observatory, Leiden University, Niels Bohrweg 2, NL-2333CA, Leiden, The Netherlands*
[13] *Department of Astronomy, University of Cape Town, Private Bag X3, Rondebosch 7701, Republic of South Africa*
[14] *INAF, Istituto di Radio Astronomia, Via Piero Gobetti, 41029, Bologna*
[15] *Research School of Astronomy and Astrophysics, Australian National University, Canberra, ACT 2611, Australia.*
[16] *Raman Research Institute, Bangalore 560080, India*
[17] *International Centre for Radio Astronomy Research (ICRAR), University of Western Australia, Crawley, WA 6009, Australia*
[18] *Dunlap Institute for Astronomy & Astrophysics, University of Toronto, 50 St George St, Toronto, ON, M5S 3H4, Canada*
[19] *School of Chemical & Physical Sciences, Victoria University of Wellington, Wellington 6140, New Zealand*

arXiv:1611.08354v1 [astro-ph.GA] 25 Nov 2016

April 2016

ABSTRACT

We present a search for transient and highly variable sources at low radio frequencies (150–200 MHz) that explores long timescales of 1–3 years. We conducted this search by comparing the TIFR GMRT Sky Survey Alternative Data Release 1 (TGSS ADR1) and the GaLactic and Extragalactic All-sky Murchison Widefield Array (GLEAM) survey catalogues. To account for the different completeness thresholds in the individual surveys, we searched for compact GLEAM sources above a flux density limit of 100 mJy that were not present in the TGSS ADR1; and also for compact TGSS ADR1 sources above a flux density limit of 200 mJy that had no counterpart in GLEAM. From a total sample of 234 333 GLEAM sources and 275 612 TGSS ADR1 sources in the overlap region between the two surveys, there were 99 658 GLEAM sources and 38 978 TGSS ADR sources that passed our flux density cutoff and compactness criteria. Analysis of these sources resulted in three candidate transient sources. Further analysis ruled out two candidates as imaging artefacts. We analyse the third candidate and show it is likely to be real, with a flux density of 182 ± 26 mJy at 147.5 MHz. This gives a transient surface density of $\rho = (6.2 \pm 6) \times 10^{-5}$ deg^{-2}. We present initial follow-up observations and discuss possible causes for this candidate. The small number of spurious sources from this search demonstrates the high reliability of these two new low-frequency radio catalogues.

Key words: radio continuum: general — catalogues — galaxies: active

1 INTRODUCTION

There are a range of astronomical phenomena that are known to be transient or highly variable at low frequencies (< 1 GHz). For example, flares from brown dwarf stars (e.g. Berger 2006; Jaeger et al. 2011), flares from Jupiter (Zarka et al. 2001), and by extension, potentially from exoplanet emission (Hess & Zarka 2011; Murphy et al. 2015), and intermittent pulsars (e.g. Sobey et al. 2015). In other cases, propagation effects such as interplanetary scintillation (e.g. Kaplan et al. 2015) can cause compact background sources such as quasars and pulsars to vary in flux density. There are also more local causes such as ionospheric distortions. Although these are typically small effects at a few hundred megahertz at the resolution of the Murchison Widefield Array (Loi et al. 2015) they can be significant for higher resolution instruments (Intema et al. 2009; van Weeren et al. 2016). The range of physical phenomena that cause radio variability is summarised by Cordes et al. (2004) and by Bowman et al. (2013) for low frequencies in particular.

Most studies of low frequency variability have targeted known objects, however there have been a small number of transients discovered through limited blind searches (e.g. Hyman et al. 2005). In recent years large-scale blind transient surveys have become possible due to new instruments such as the Long Wavelength Array (LWA1; Taylor et al. 2012), the Low Frequency Array (LOFAR; van Haarlem et al. 2013), the Murchison Widefield Array (MWA; Tingay et al. 2013) and the Jansky Very Large Array (VLA) Low Band Ionospheric and Transient Experiment (VLITE; Clarke et al. 2016). A range of low-frequency surveys for radio transients have been conducted on these instruments (e.g. Bell et al. 2014; Obenberger et al. 2015; Polisensky et al. 2016) in part as preparation for the Square Kilometre Array (SKA; e.g. Fender et al. 2015). In addition there have been a number of surveys using archival low frequency data from the Very Large Array (Jaeger et al. 2012) and Molonglo (Bannister et al. 2011) telescopes.

So far, most surveys for radio transients at low frequencies (e.g. Lazio et al. 2010; Bell et al. 2014; Polisensky et al. 2016) have not found any astrophysical sources, resulting in upper limits on the rate of transient and highly variable sources as summarised by Rowlinson et al. (2016). However, there are a few surveys that have resulted in detections. One is the archival search of 325 MHz Very Large Array observations by Jaeger et al. (2012). They found a single candidate in 72 hours of observations in the Spitzer-Space-Telescope Wide-area Infrared Extragalactic Survey (SWIRE) Deep Field. This source was detected over a 6 hour period with a flux density of 1.70 ± 0.25 mJy. Another example is the recent result by Stewart et al. (2016) who found a single candidate astrophysical transient in 400 hr of LOFAR monitoring of the North Celestial Pole. Their candidate had a duration of a few minutes and a 60 MHz flux density of $15 - 25$ Jy. The nature of this object is still unknown, but it suggests that we might now be approaching the survey parameters required to detect low-frequency radio transients in blind surveys. Metzger et al. (2015) present model predictions for the rates of extragalactic synchrotron transients which are significantly lower than the rates that current low-frequency blind surveys probe. However, these do not cover all the classes of objects we expect to see at low frequencies, in particular Galactic objects or coherent emitters such as intermittent pulsars.

In this paper we present a search for radio transients at ~ 150 MHz, over typical timescales of three years, to a flux density cutoff of 100–200 mJy. We conducted the search using the GLEAM survey (Wayth et al. 2015) survey and the first Alternative Data Release of the 150 MHz TIFR GMRT Sky Survey (TGSS ADR1; Intema et al. 2016). Unless stated otherwise, all flux density limits are at 3σ confidence.

2 DATA ANALYSIS

2.1 The GLEAM Survey

The Murchison Widefield Array (Tingay et al. 2013) is a 128-tile low-frequency radio interferometer located in Western Australia. One of the major MWA projects is GLEAM: The GaLactic and Extragalactic All-sky MWA survey (Wayth et al. 2015). GLEAM is a survey of the radio sky south of declination $+30^\circ$ at frequencies between 72 and 231 MHz. The observations used in this work were carried out between 2013 June and 2014 July. At 154 MHz the image resolution is approximately $2.5' \times 2.2'/\cos(\delta + 26.7^\circ)$. The typical sensitivity of GLEAM snapshot images ranges from 40 to 200 mJy beam^{-1} between 231 MHz and 72 MHz respectively. The final catalogue is 92.6% complete at 200 mJy and 79.5% complete at 100 mJy.

The observation and data reduction strategy for GLEAM is described in detail by Hurley-Walker et al. (2016).

2.2 The TGSS ADR1 Survey

The Giant Metrewave Radio Telescope (GMRT; Swarup 1990) is an array of 30 antennas, each with a diameter of 45 m. The GMRT has a maximum baseline of 25 km and operates at frequencies between 150 and 1500 MHz. Between 2011 April and 2012 March the GMRT was used to carry out a 150 MHz survey of the sky north of declination $\delta = -55^\circ$.

Until recently, the bulk of the data collected by the TGSS was unpublished. Motivated by recent improvements in low-frequency calibration and imaging, Intema et al. (2016) have re-processed the TGSS observations and released both the resulting Stokes I continuum images and a catalog of 620 000 radio sources down to the 7σ level (TGSS ADR1). The TGSS ADR1 data release covers the sky north of declination $\delta = -53^\circ$, excluding the most southern (lowest elevation) pointings. The images have a median RMS of 3.5 mJy beam^{-1} and an approximate resolution of $25'' \times 25''$ or $25'' \times 25''/\cos(\delta - 19)^\circ$ for declinations south of $\delta = +19^\circ$.

2.3 Search strategy

We conducted our search using the GLEAM first data release catalogue (Hurley-Walker et al. 2016) and the TGSS ADR1 7-sigma source catalog (Intema et al. 2016). The two surveys cover a common area of sky between $-53^\circ \leqslant \delta \leqslant +30^\circ$. The GLEAM survey has significantly lower completeness above $\delta = +10^\circ$ so we excluded these northern declinations from our comparison. The GLEAM catalogue excludes

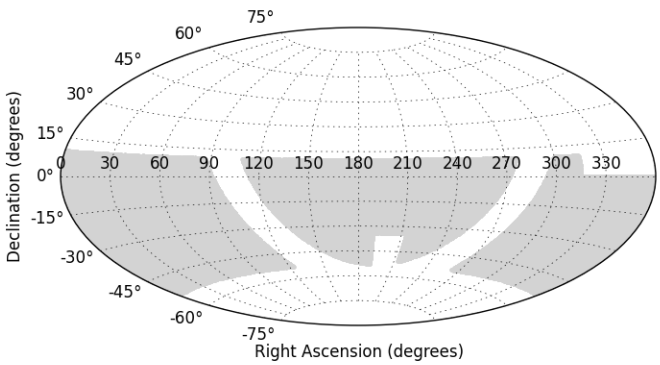

Figure 1. The sky coverage of our survey (in Aitoff projection); the grey shaded area shows the overlap region between GLEAM and TGSS, excluding the sky north of $\delta = 10^\circ$. The masked regions, described in the text, are shown in white.

the Galactic plane region $|b| < 10^\circ$ and a 1289 sq deg area centred on 22.5^h, $+15^\circ$ that was ionospherically distorted. There are also several small regions that are masked around the bright radio galaxy Centaurus A. Figure 1 shows the regions used for the analysis in this paper; the total area surveyed is 16 230 sq deg (39.3% of the sky).

On average the TGSS observations took place about three years before the GLEAM survey observations. The GLEAM survey includes a sub-band centred on 154 MHz, which is close to the TGSS frequency of 150 MHz, so they are well matched. Due to the different properties of these surveys, as discussed below, we searched for transients using two approaches. We crossmatched sources in the GLEAM survey with TGSS, and looked for those with no match, and we crossmatched sources in TGSS with the GLEAM catalogue and looked for sources with no match.

In conducting these searches there are two main differences between the survey catalogues that need to be accounted for (i) the sensitivity limit and completeness of GLEAM compared to TGSS; and (ii) the lower resolution of GLEAM compared to TGSS.

(i) The typical RMS sensitivity of TGSS is $3.5\,\mathrm{mJy\,beam^{-1}}$, and the TGSS catalogue was constructed using a 7σ source-finding cutoff, which gives a limiting flux density of 24.5 mJy. The GLEAM survey is less sensitive; the catalogue is 92.6% complete at 200 mJy, whereas TGSS is close to 100% complete at 200 mJy. To account for this we used a relatively high flux density cutoff of 100 mJy for our GLEAM to TGSS comparison. For the reverse comparison we applied a flux density cutoff of 200 mJy to the TGSS sources, to avoid false positive transient candidates due to incompleteness in the GLEAM survey.

(ii) The resolution of the TGSS is $25'' \times 25''$ for $\delta > 19^\circ$ and $25'' \times 25''/\cos(\delta - 19^\circ)$ for $\delta < 19^\circ$, compared to $2.5' \times 2.2'/\cos(\delta + 26.7^\circ)$ for GLEAM. The lower resolution of GLEAM means we would expect to see a significant number of objects that have extended emission that is resolved out in TGSS, which produces a large number of false positives when crossmatching GLEAM to TGSS. A related issue is multi-component radio galaxies in which the catalogued position is offset between the two catalogues.

We addressed these issues firstly by restricting the crossmatch sample to sources that were compact in GLEAM (using the criteria discussed in Section 3.1); and secondly by searching for GLEAM sources that had no match in TGSS or in three archival catalogues: the NRAO VLA Sky Survey (NVSS, at 1.4 GHz; Condon et al. 1998); the Sydney University Molonglo Sky Survey (SUMSS, at 843 MHz; Mauch et al. 2003); and the VLA Low Frequency Sky Survey, redux (VLSSr, at 74 MHz; Lane et al. 2014).

2.4 Flux density scale

Before we conducted our search we checked that the flux density scales of the two catalogues were aligned. To do this we selected bright sources (> 900 mJy) in our survey region that were compact in both GLEAM (using the criterion $(a \times b)/(a_{\rm psf} \times b_{\rm psf}) < 1.1$ where a and b are the major and minor axis of a Gaussian fit to the source) and TGSS (using the criterion that the object was fit by a single Gaussian).

We cross-matched these objects, and compared their flux densities as shown in Figure 2. We fit these data using orthogonal distance regression, with the uncertainty in $S_{\rm TGSS}$ and $S_{\rm GLEAM}$ as weights. The uncertainty on $S_{\rm GLEAM}$ was the RMS noise combined in quadrature with the systematic uncertainty. For the ~ 3000 sources plotted, the best fit ratio of TGSS/GLEAM was 0.97, demonstrating the systematic difference between the measured flux densities in these catalogues is $\sim$3%. This difference is to be expected since the GLEAM survey is on the Baars et al. (1977) flux density scale, while TGSS is on the Scaife & Heald (2012) flux density scale.

Although the overall agreement is good, there is some scatter around the mean ratio, with a small fraction of sources showing significantly different flux densities in both surveys. The likely cause of these differences is a combination of the difference in resolution between the two surveys; the better low surface brightness sensitivity of GLEAM; errors in the local calibration and flux scale in each survey; and some variability in the source population. In particular the flux scale agreement is different in different regions of the sky: we discuss this further in Section 3.2.1.

3 RESULTS

3.1 GLEAM to TGSS comparison

There are a total of 234 333 GLEAM catalogue sources in the overlap region between the two surveys. We did an initial exploration of the data by cross-matching the GLEAM catalogue with the TGSS, SUMSS, NVSS and VLSSr catalogues, and visually inspecting all GLEAM sources that did not have a match in any of these catalogues (a total of 2 219 sources). A majority of these sources were either extended, or had a match in the survey images that was below the formal catalogue limits for a given survey.

From this exploration we developed the criteria below to search for GLEAM sources that had no TGSS counterpart:

(i) Applied a GLEAM 200 MHz flux density cutoff of 100 mJy (*leaving 133 686 sources*);

(ii) Excluded sources that were extended in GLEAM, using the criterion $(a \times b)/(a_{psf} \times b_{psf}) \geqslant 1.1$ where a and b

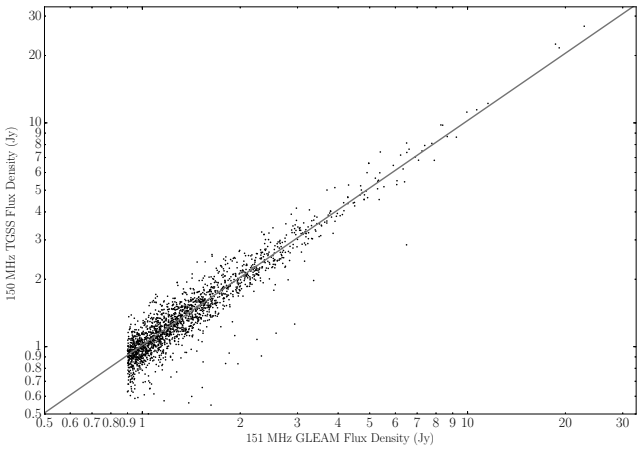

Figure 2. TGSS 150 MHz flux density versus the GLEAM 151 MHz sub-band flux density for bright, compact sources in our survey area. The line of best fit, shown as a solid line, gives a TGSS/GLEAM flux density ratio of 0.97.

are the major and minor axis of a Gaussian fit to the source (*leaving 99 658 sources*);

(iii) Cross-matched the GLEAM catalogue with the TGSS catalogue, using a search radius of 1.0′ and selected sources with no match (*leaving 1 371 sources*);

(iv) Cross-matched the sources with no TGSS counterpart with the SUMSS, NVSS and VLSSr catalogues, using a search radius of 2.5′ and selected sources with no match (*leaving 15 sources*);

(v) Visually inspected the sources and excluded a small number of sources that were GLEAM processing artefacts.

This resulted in two candidate transients above our 100 mJy limit, GLEAM J153424−114947 and GLEAM J153653−115052, which we discuss below.

The sources that did not have a match in the TGSS catalogue, but that did have a counterpart in NVSS or SUMSS (excluded in step (iv) above) were typically multiple-component radio galaxies. These were unresolved in GLEAM, but resolved into multiple components in TGSS, and hence had a catalogued position or positions that were more than 1.0′ from the GLEAM position.

The small number of GLEAM imaging artefacts that we discovered in the manual inspection process have now been removed from the final GLEAM catalogue.

3.1.1 Analysis of GLEAM candidates

GLEAM J153424−114947 has a 200 MHz flux density of 204 ± 10 mJy. There is no detection in TGSS, with a 3σ limit of 8.4 mJy beam^{-1}. There are no detections in the VLSSr (3σ limit of 330 mJy beam^{-1}) or NVSS (3σ limit of 1.4 mJy beam^{-1}) surveys.

GLEAM J153653−115052 has a 200 MHz flux density of 134 ± 10 mJy. There is no detection in TGSS, with a 3σ limit of 6.2 mJy beam^{-1}. There are no detections in the VLSSr (3σ limit of 231 mJy beam^{-1}) or NVSS (3σ limit of 1.3 mJy beam^{-1}) surveys.

These detections appeared to be robust (no sign of nearby bright sources or other apparent causes), however their close proximity on the sky raised concerns and so we inspected the individual snapshot images from which the GLEAM mosaics are constructed. In the snapshot images, each source only appears only in one image. We realized from examination of these and at least six additional snapshot images that there was just a single source that appeared to move across the sky with time, shifting by approximately 0.°6 in right ascension between adjacent images taken 10 min apart, with minimal motion in declination. The source is very close to the edge of the images ($y > 3880$, with an image size of 4000 pixels) in the region where deconvolution is disabled.

We reprocessed the individual snapshot images using different imaging parameters: we used the same pixel scale of 25.″2 pixel^{-1}, but with an image size of 6144 pixels. This meant that the imaged area was 43° compared to 30.°34, and the source was only 85% of the way to the edge rather than 97%. Otherwise the imaging parameters were similar. We found no source at the position of GLEAM J153424−114947 or GLEAM J153653−115052 in either of the reprocessed snapshots where they previously appeared (see the right hand panels of Figure 3), while the other sources remained, demonstrating that the potential transients are likely to be imaging artefacts. The most likely explanation is that they are a form of aliasing in which a bright source outside the field has been aliased in.

3.1.2 GLEAM artefacts

As a result of this analysis these two candidates were established as artefacts and removed from the main GLEAM catalogue. In the GLEAM pipeline processing the primary field-of-view is imaged down to at least 10% of the primary beam, leaving, for every observation, approximately 100 square degrees of sky with a primary beam response between 0−10% outside the imaged field-of-view. The 7 brightest sources in the sky are peeled where possible, but in two cases, the sources could not be peeled due to contamination from other bright sources. In one observation, Hercules A lay just outside the field-of-view, and was not peeled, due to the confounding presence of 3C353 in a side lobe, resulting in an alias inside the imaged field-of-view. In 19 further cases, Centaurus A could not be peeled due to contamination from the Galactic Plane, resulting in 19 further aliases. These were manually removed from the final catalogue. For images which form the source-detection mosaics across 170–231 MHz, all other cases of potential unpeeled source contamination were checked and no aliases were found. There are a small number of aliases in the lower-frequency mosaics, but these are not used for source-finding, and the aliases do not coincide with other sources.

It is possible that sources of flux densities comparable to 3C444 ($S_{200\mathrm{MHz}} \approx 60$ Jy), the faintest peeled source, could be just outside the field of view and cause aliases inside it. However, the chances of this are very small, as the source must lie at a Declination within five degrees of one of the GLEAM pointing centres, in order to fall on an image edge rather than a corner, and fall just outside the field-of-view. Because the GLEAM mosaics are formed by weighting snapshots by the square of their primary beam responses, the contribution of such an alias to the mosaic would be downweighted by at least a factor of 100, effectively reducing its flux density by that factor. Therefore, we do not expect

sources fainter than 3C444 to contribute detectable sources to the mosaics, as they would appear with $S < 6$ mJy, which is below the detection limit across the sky.

Hence, as a result of the extensive quality control done as part of the GLEAM survey, we do not think it is likely that similar artefacts would have a significant impact on the overall reliability of the GLEAM catalogue.

3.2 TGSS to GLEAM comparison

There were a total of 275 612 TGSS sources in our survey region. To do the reverse comparison, crossmatching TGSS sources with GLEAM, we followed the steps below:

(i) Selected TGSS sources above 200 mJy (*leaving 74 876 sources*);
(ii) Selected compact sources by choosing those that were fit by a single Gaussian, marked 'S' in the TGSS ADR1 catalogue (*leaving 38 978 sources*);
(iii) Crossmatched these with the GLEAM catalogue, using a radius of $1'$ and selected sources with no match (*leaving 640 sources*);
(iv) Visually inspected all sources with no match and excluding those that were multi-component sources (generally double and triple radio galaxies) that are resolved in TGSS but not in GLEAM;
(v) Excluded sources that are in regions of poor image quality in the TGSS mosaics.

This resulted in a single candidate transient, TGSSADR J183304.4−384046, which we discuss below.

3.2.1 Analysis of the TGSS candidate

TGSSADR J183304.4−384046 has a 150 MHz flux density of 304 mJy, but was not detected in GLEAM (3σ limit of 41 mJy beam^{-1}), SUMSS (3σ limit of 4.9 mJy beam^{-1}), NVSS (3σ limit of 1.4 mJy beam^{-1}) or AT20G (3σ limit of 30 mJy beam^{-1}). We also searched archival radio surveys ATPMN (McConnell et al. 2012) and the Molonglo 408 MHz survey (Hunstead, private communication) and found no detections. These limits are summarised in Table 1 and Figure 4. We did not detect the source in any of the 20 GLEAM sub-bands, and we have included 4 representative sub-band limits on the flux density in the table and SED. The TGSS and GLEAM images are shown in Figure 5.

Based on these non-detections we observed this source with the Australia Telescope Compact Array on 2016 April 1. We had a total time of 1.5 hours on source at each of 2.1, 5.0 and 9.0 GHz in the H214 array. We did not see any emission at the position of TGSSADR J183304.4−384046, obtaining limits of 0.75 mJy beam^{-1} at 2.1 GHz, 0.24 mJy beam^{-1} at 5 GHz and 0.045 mJy beam^{-1} at 9 GHz. This suggested the source was either a transient that had faded since the TGSS observations, or an artefact.

We considered the possibility that this source was an imaging artefact from the TGSS processing, for example a CLEAN artefact caused by the bright source approximately $6'$ to the south west. This neighbouring source has a GLEAM 151 MHz flux density of 1.75 ± 0.04 Jy (GLEAM J183318−384608), and a 147.5 MHz flux density of 3.0 ± 0.3 Jy (TGSSADR J183317.7−384613) in the TGSS ADR1.

The significant difference in the measured flux density of this neighbouring source led us to do further analysis of the flux density scale in the region of the transient candidate. We selected all bright compact sources within a 1 degree radius of the candidate and found the mean flux ratio of the

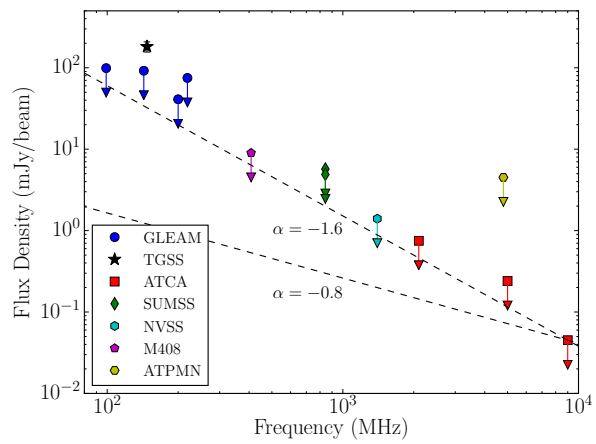

Figure 4. Radio spectral energy distribution (SED) of TGSSADR J183304.4−384046, based on the data in Table 1. We have used the scaled TGSS flux density, as discussed in the main text. Note that these are not based on contemporaneous observations. For the presumed quiescent emission (ignoring the TGSS detection), the most constraining measurement for typical spectral indices is the ATCA 9 GHz observation. We show model SEDs for spectral indices of $\alpha = -0.8$ (typical for extragalactic GLEAM sources; Hurley-Walker et al. 2016) and $\alpha = -1.6$ (the steepest spectral index that matches all of the limits).

Table 1. Summary of radio measurements and limits for TGSSADR J183304.4−384046.

Survey	Freq (MHz)	Date	S† (mJy/bm)	Ref
GLEAM	99	2014 Jun 09	< 99	*
GLEAM	143	2014 Jun 09	< 92	*
TGSS	147.5	2011 Apr 27	182 ± 26‡	I16
GLEAM	200	2014 Jun 09	< 41	*
GLEAM	219	2014 Jun 09	< 75	*
M408	408	1972 Jul 15	< 9	Hpc
SUMSS	843	2005 Aug 03	< 5.7	M03
SUMSS	843	2006 Mar 09	< 4.9	M03
NVSS	1400	1993 Oct 07	< 1.4	C98
ATCA	2100	2016 Apr 01	< 0.75	*
ATPMN	4800	1994 Mar 14	< 4.5	M12
ATCA	5000	2016 Apr 01	< 0.24	*
ATCA	9000	2016 Apr 01	< 0.045	*
AT20G	20 000	2004 Aug 11	< 30	H11

† Flux density or 3σ upper limits.
‡ See Section 3.2.1 for discussion of the flux scale.
References: * (This work), C98 (Condon et al. 1998), Hpc (Hunstead, private communication), H11 (Hancock et al. 2011), I16 (Intema et al. 2016), M03 (Mauch et al. 2003), M12 (McConnell et al. 2012)

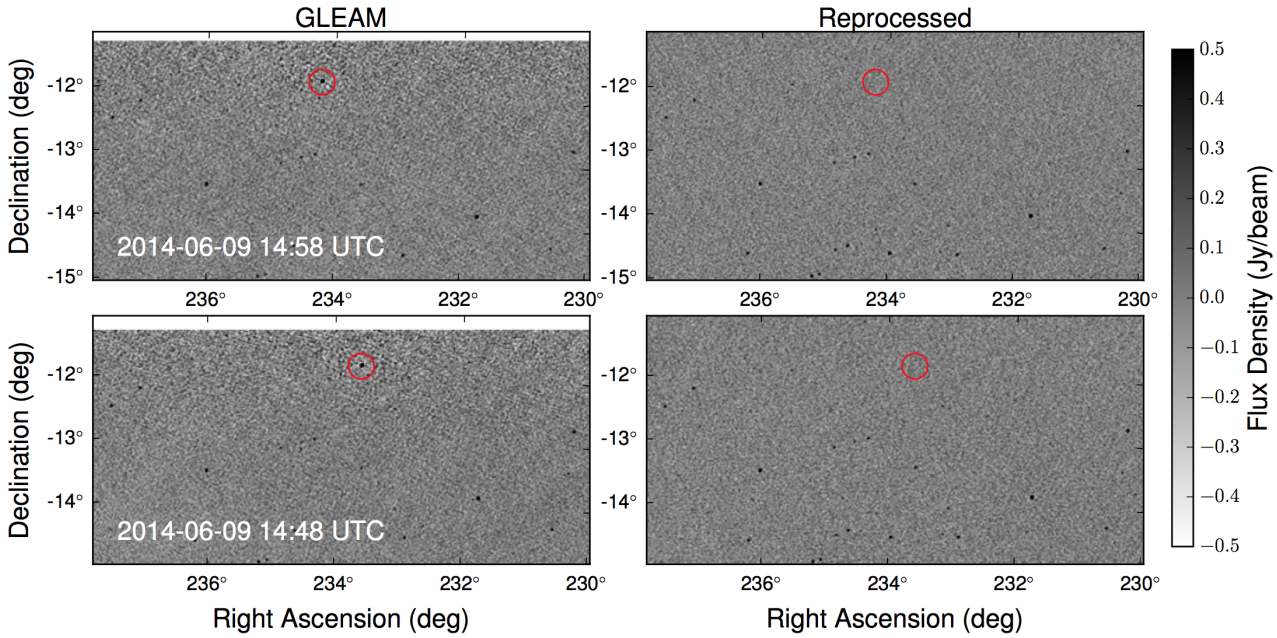

Figure 3. *Left:* GLEAM snapshot images showing the two transient candidates GLEAM J153424−114947 and GLEAM J153653−115052. *Right:* The reprocessed images in which the candidates no longer appear, demonstrating that these are imaging artefacts.

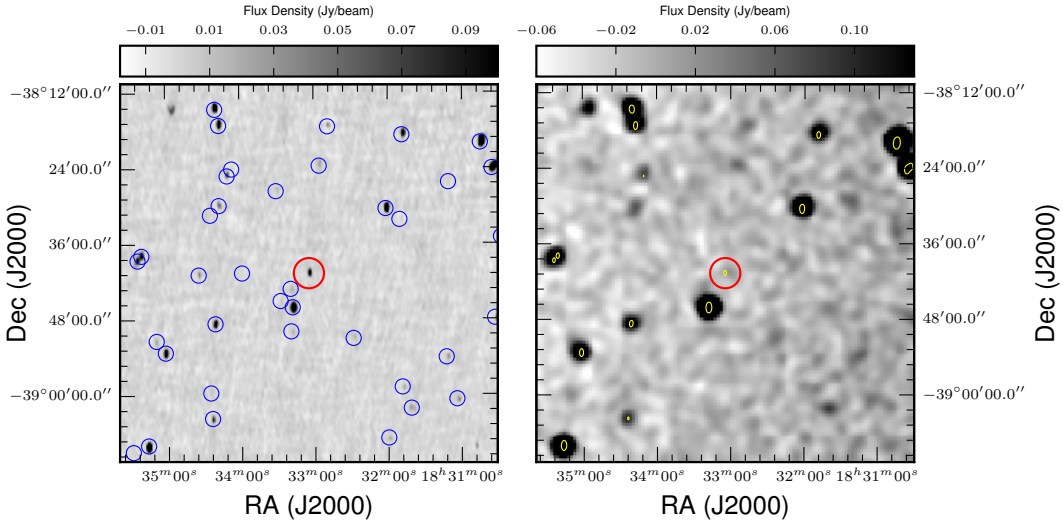

Figure 5. TGSS ADR1 (left) and GLEAM (right) images of the transient candidate TGSSADR J183304.4−384046 (shown with a red circle). On the TGSS ADR1 image, the blue circles show the location of NVSS sources with a 1.4 GHz flux density greater than 5 mJy. The GLEAM image is overlaid with a TGSS contour at 80 mJy beam^{-1} to show the position of TGSS sources.

GLEAM 151 MHz flux density to the TGSS 147.5 MHz flux density was 0.6. This is due to flux scale uncertainties in the TGSS ADR that are currently being rectified. Based on this analysis, the flux density of the candidate transient may be $0.6 \times 304 = 182 \pm 26$ mJy rather than the catalogued value. We have used this scaled value in the spectral energy distribution in Figure 4. We have also scaled the TGSS image in Figure 5 by a factor of 0.6. We estimate that this scaling has an additional uncertainty of 10% based on the scatter of the flux ratios.

We looked at the uncombined TGSS pointing images, before primary beam correction and found that the transient candidate appears in two images (R56D08 and R57D09). These pointings were observed on the same night, but with slightly different *uv*-coverage. Each pointing was processed independently. Although the transient candidate is well beyond the half-power point of the primary beam in image R57D09, it is still clearly visible, which makes it unlikely to be an artefact. In addition, we did not find evidence of similar artefacts around other sources of similar brightness to

this candidate's neighbour, making it unlikely that the candidate is a result of the CLEAN process. Finally, Figure 5 shows that much fainter sources in the same region have matches in NVSS (blue circles) demonstrating the high image fidelity. Hence after this analysis we concluded that the transient is likely to be real.

3.2.2 Multi-wavelength Search

We found no obvious infrared counterparts in the four *Wide-field Infrared Survey Explorer* (*WISE*; Wright et al. 2010) bands (see Figure 6) or in the three 2-Micron All-Sky Survey (2MASS; Skrutskie et al. 2006) bands, with $5\,\sigma$ upper limits in Table 2. We also found no likely counterparts in SIMBAD and NED searches. The position of the source rules out solar system planets.

We observed the location of TGSSADR J183304.4−384046 with the 1.3 m SkyMapper survey telescope (Keller et al. 2007) on 2016 April 07, with 3×100 s exposures in the g filter, 5×100 s exposures in the r filter, and 10×100 s exposures in the i filter. The seeing was about $2\farcs5$ in all bands. The data were processed with the standard SkyMapper pipeline and the individual images coadded. As shown in Figure 6, we see only a single source within the $3\,\sigma$ radius ($6''$) error circle, down to $5\,\sigma$ limiting depths of 21 mag in all bands. The source appears unresolved, and has $g > 21$, $r = 19.80 \pm 0.07$, and $i = 18.73 \pm 0.03$ (Table 2). Using the extinction model of Drimmel et al. (2003) we estimate the extinction to be $A_V \approx 0.5$ mag for distances $\gtrsim 1$ kpc.

4 DISCUSSION

4.1 Interpretation of TGSSADR J183304.4−384046

There are a number of possible interpretations of this object, which we will briefly discuss here. Further analysis is left for follow-up work once more observations have been conducted.

We have a single detection of this source, at 182 ± 26 mJy at 147.5 MHz. The non-detection in GLEAM 3 years later implies the source has at least faded to $<$ 41 mJy beam^{-1}. We show the spectral energy distribution in Figure 4. Assuming a typical spectral index of $\alpha = -0.8$ (where $S_\nu \propto \nu^\alpha$), the non-detection with the ATCA at 9 GHz implies a 151 MHz flux density of 1.2 mJy, which would require considerably deeper observations to confirm.

The Galactic latitude of $b = -13.2°$ means we must consider both Galactic and extragalactic origins for TGSSADR J183304.4−384046. We can estimate the brightness temperature T_B for both scenarios: assuming variability on timescales of $\sim$ 1 yr and no relativistic beaming, we find $T_B \approx 3000\,K$ at a distance of 1 kpc (Galactic), or $T_B \approx 3 \times 10^{15}$ K at a distance of 1 Gpc (extragalactic). The former is consistent with a wide range of progenitors. In contrast, the latter exceeds the 10^{12} K limit (Readhead 1994), suggesting that if extragalactic the source is relativistic or the variability is not intrinsic.

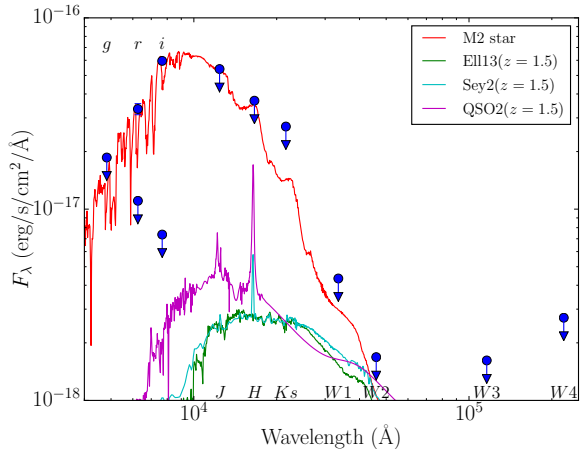

Figure 7. Optical/infrared spectral energy distribution of TGSSADR J183304.4−384046, based on our SkyMapper g, r, and i data long with archival 2MASS and *WISE* upper limits (Tab. 2). We show both the detected r and i measurements of the potential stellar source from Fig. 6 as well as upper limits for the rest of the error region. We show a reddened M2 star from Castelli & Kurucz (2004) at a distance of 1.1 kpc (red curve), which passes through the r and i detections. We also show an early-type galaxy (model "Ell13"; green curve), a Seyfert galaxy (model "Sey2"; cyan curve), and a QSO (model "QSO2"; magenta curve) from Polletta et al. (2007), all at redshift of 1.5 and normalized to $K_s = 18$ mag (following the $K - z$ relation of Willott et al. 2003).

4.1.1 Galactic source types

At low frequencies, most potential Galactic transients emit via coherent processes that exhibit variability on short timescales of seconds, minutes or hours: for example, giant pulses from pulsars, intermittent pulsars or flares from cool stars or exoplanets (e.g., Bowman et al. 2013). For example, to have coherent emission with brightness temperature $> 10^{12}$ K would require emission on timescales $\lesssim 2000$ s. Given the timescales our search probes (15 min for the TGSS observations, and a few hours for GLEAM), discovering a source with such short timescale variability would be very unlikely unless the duty cycle were quite large, and the unknown timescale also means that any limits on brightness temperature are unconstraining.

If the optical source from § 3.2.2 is not the counterpart of TGSSADR J183304.4−384046, we can exclude a range of stellar (Covey et al. 2007) or sub-stellar (Hawley et al. 2002) counterparts. Main-sequence stars with spectral types earlier than G8 can be excluded out to distances $\gtrsim 20$ kpc, and even stars as late as M6 can be excluded out to 1 kpc. Brown dwarfs can be excluded to distances of almost 1 kpc (late M/early L) down to ≈ 10 pc (late L/early T).

If the source is the counterpart, the $r - i$ color implies a spectral type of roughly M2 at a distance of about 1 kpc. This is largely consistent with the 2MASS near-infrared upper limits (Fig. 7). Such an association is plausible: while most low radio frequency observations of the lowest-mass stars and brown dwarfs have not seen any emission to much deeper limits (e.g., Jaeger et al. 2011), bright, short-duration flares have been seen from some higher mass M-dwarf stars (e.g., Spangler & Moffett 1976). If a stellar flare, the implied

Table 2. Summary of optical and IR measurements for TGSSADR J183304.4−384046.

	SkyMapper*			2MASS†			*WISE*‡			
Filter	g	r	i	J	H	K_s	W1	W2	W3	W4
Wavelength (μm)	0.48	0.63	0.77	1.24	1.66	2.16	3.35	4.60	11.6	22.1
Magnitude	> 21	$19.80 \pm 0.07^{\S}$	$18.73 \pm 0.03^{\S}$	> 16.9	> 16.2	> 15.5	> 15.7	> 15.4	> 11.6	> 8.2
Flux Density (μJy)	< 14	$44 \pm 3^{\S}$	$117 \pm 3^{\S}$	< 277	< 339	< 421	< 162	< 119	< 726	< 4408

∗ Magnitudes are defined on the AB system.
† Magnitudes are defined on the Vega system.
‡ Magnitudes are defined on the Vega system.
§ Assuming the source discussed in the text is the counterpart. If not, the source is $r > 21$ and $i > 21$, or $F_\nu, r < 15\,\mu$Jy and $F_\nu, i < 15\,\mu$Jy.

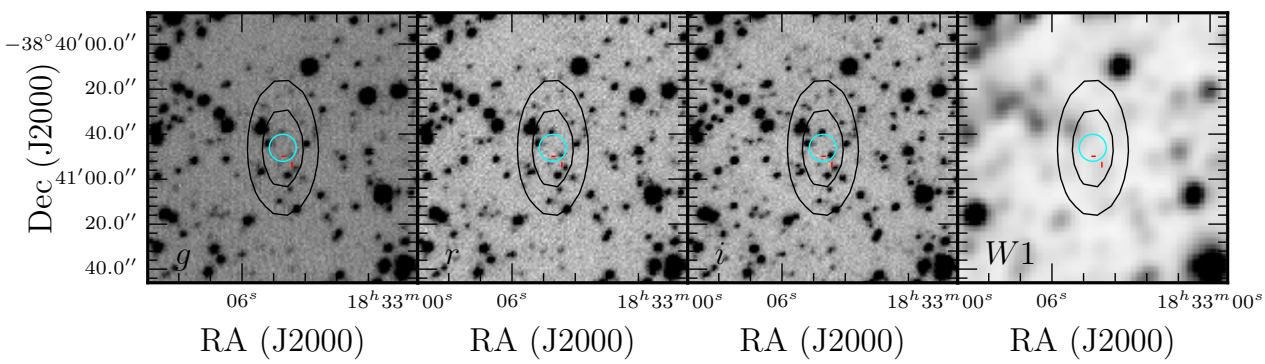

Figure 6. Multi-wavelength images of TGSSADR J183304.4−384046, showing SkyMapper g, r, and i from left to right, along with *WISE* $W1$ at the right. All images show the same field-of-view. The contours mark 100 mJy beam^{-1} and 200 mJy beam^{-1}. The cyan circles show the 3σ radius ($6''$) region searched for counterparts, and the ticks mark the single stellar source identified within that region.

luminosity density is about 4×10^{20} erg s^{-1} Hz^{-1}, which is not out of line with observed flares (e.g., Nelson et al. 1979). Yet given the flare rates of even the most active M dwarfs, and assuming the probability of burst emission follows Poisson statistics, the likelihood of observing a flare in the 15 minute TGSS observation is low (<20%) (Abada-Simon & Aubier 1997), and it is even more unlikely given the lack of flaring in the multiple epochs of MWA data we investigated. In addition, this source is otherwise undistinguished, and we find a density of sources with $i < 18.7$ of 0.0035 arcsec^{-2} implying 0.4 sources within $6''$ by chance. Searches for further flares from this source as well as more detailed investigations of the potential stellar counterpart are needed.

Another possibility is coherent emission from the magnetosphere of a Jupiter-like exoplanet (Zarka et al. 2001). The frequency of this type of emission is strongly tied to the magnetic field strength of the planet's magnetosphere: emission at 150 MHz implies a magnetic field of about 50 G. Therefore, the observed radio emission could extend over a small bandwidth and explain the non-detections at higher frequencies. However, recent modeling of the radio emission expected from Jupiter-like exoplanets predict flux densities of a few mJy (Fujii et al. 2016; Grießmeier et al. 2011), several orders of magnitude lower than the flux density measured for TGSSADR J183304.4−384046.

4.1.2 Extragalactic source types

In contrast to the Galactic sources, the sources expected to appear or disappear on the yearly timescales we probed in this survey are most likely to be extragalactic synchrotron sources, such as afterglows from gamma-ray bursts or tidal disruption events, which tend to be relatively faint at low frequencies (Burlon et al. 2015; Metzger et al. 2015). Note that synchrotron emission is also seen from Galactic X-ray binaries (e.g., Fender 2006), but the lack of any high-energy counterpart makes this very unlikely.

The best predictions for the rates of extragalactic synchrotron transients are given by Metzger et al. (2015). For flux densities normalised to $z \approx 0.55$, all the main categories of sources they consider (short gamma-ray bursts, long gamma-ray bursts, radio supernova, tidal disruption events and neutron star mergers) are expected to have flux densities of less than 0.1 mJy on timescales of 1 to 3 years. Note that we do not see any gamma-ray burst from either *Swift* or *Fermi* with a position consistent with TGSSADR J183304.4−384046. If the object we have detected is an extragalactic synchrotron source this could suggest a higher rate of these sources than predicted by Metzger et al. (2015).

Another possibility is that the emission we see is related to an active galaxy, either intrinsic variability from an AGN flare (e.g., Hughes et al. 1992; Croft et al. 2013; Bignall et al. 2015) or extrinsic variability caused by interstellar scintillation. Given the large modulation implied by the GLEAM

upper limit and the non-detections at other radio frequencies we can rule out refractive scintillation as the origin of the variability, but diffractive scintillation is possible. The NE2001 electron density model (Cordes & Lazio 2002) predicts a scintillation bandwidth of < 0.1 kHz at 150 MHz, suggesting that any scintillations are likely to be washed out. Scintillation by discrete structures like Extreme Scattering Events (e.g. Fiedler et al. 1987) is still possible, but the degree of modulation needed to accomodate our 9 GHz limits with a standard extragalactic SED (roughly 10) is significantly higher than is seen in most ESEs (~ 2).

Assuming an extragalactic origin, we can use the photometry in Table 2 to put limits on the host galaxy. Radio-loud AGN tend to be hosted by massive galaxies, and follow a rather tight relationship between K-magnitude and redshift (Willott et al. 2003). To be consistent with all of our data and upper limits requires models with $K \gtrsim 18$ (Fig. 7), which implies $z \gtrsim 1.5$ for typical (few $L_\star$) AGN hosts. The *WISE* W1 photometry is suggestive of a similar lower bound in redshift (Gürkan et al. 2014), and the optical upper limits are also consistent with a radio-loud AGN at moderate to high redshift (Stern et al. 2012). Overall we see a consistent interpretation as a $z \sim 1.5$ radio galaxy somewhat above the break in the radio luminosity function (Vardoulaki et al. 2010), although a less massive host could be at somewhat lower redshift. Deeper near-IR imaging could help to identify any host galaxy, and deeper radio imaging could be used to search for a quiescent counterpart.

We plan to conduct further follow-up observations to establish whether our candidate is an extragalactic synchrotron source. For example, we would expect to detect the quiescent emission of a flaring AGN with deeper radio observations, or the host galaxy of a gamma-ray burst or supernovae with deeper optical and infrared observations.

4.2 Transient rates

The total area covered by our search is 16 230 sq deg. We detected a single transient above 100 mJy over this area, which results in a surface density estimate of $\rho = (6.2 \pm 6) \times 10^{-5}$ deg^{-2}. Figure 8 shows our new result (red star) compared to other results from the literature. The timescales explored by our survey range from 1 to 3 years (TGSS was conducted between 2011 April and 2012 March, and GLEAM was conducted between 2013 June and 2014 July). To accommodate this uncertainty we have plotted our point at 2 years, with an error bar of ± 1 year.

In terms of long timescales, the best limits in the literature are by Rowlinson et al. (2016) who found a surface density of $\rho < 6.6 \times 10^{-3}$ deg^{-2} on yearly timescales. Our detection is an order of magnitude lower than this and so is consistent with previous results. To date, most low-frequency surveys have been limited in sensitivity, something the expanded MWA, the JVLA and LOFAR will help overcome.

Figure 8 also shows the predicted rates for a range of phenomena, as calculated by Metzger et al. (2015). The coloured lines show the sky density of sources above flux density F_ν for frequency $\nu = 150$ MHz. We have included a selection of results from Figure 3 in Metzger et al. (2015), specifically: magnetars (blue); off-axis tidal disruption events (red); long GRBs with $\theta_{\rm obs} = 1.57$ (green); off-axis short GRBs (orange); and neutron star merger leaving black hole (black). See Metzger et al. (2015) for a detailed description of how these model predictions were calculated, and their associated uncertainties, which can be up to an order of magnitude. From plot we can see that our current results and the limits set by Rowlinson et al. (2016) are now approaching the point of being able to test these predictions.

4.3 Search completeness

It is possible that other transient sources were overlooked due to them being a single source at the resolution of TGSS but blended with another source at the resolution of GLEAM (in other words it is close, in sky projection, to a steady source). Alternatively, a transient source could be overlooked in our search if it occured at the same location as a persistent source: a recent example of this situation is the claimed host galaxy of a fast radio burst (Keane et al. 2016) (but see Williams & Berger 2016 for further discussion).

This would have the effect of increasing or decreasing the flux density of a GLEAM source, but it would not be detected in the analysis we have done here. To formally account for this in our transient rate calculation we could exclude the area around each unresolved GLEAM source in our survey region. This is equivalent to $A = 267\,860 \times 2.2' \times 2.5' = 409$ deg^{-2}, which is less than 3% of the survey area.

Another possibility is that some of the GLEAM sources with a TGSS match were false matches due to positional coincidence of the source in the TGSS catalogue. To evaluate this we shifted the positions of the GLEAM sources by a random offset in right ascension and declination of between 5 and 10 arc minutes. We then repeated the cross-matching with the TGSS catalogue and found that of the 99 658 compact sources above 100 mJy in our survey region, 1371 had a match. This implies that up to $\sim 1.3\%$ of the sources ruled out in our process could have been transients. However, since the total number of transients in our survey is $\ll 1$, this means that the expectation is that the number of sources we would miss due to this issue is less than one. The caveat here is that many classes of physical transient (e.g. radio supernovae) will occur at the same location as a persistent radio source (the host galaxy) and this is not accounted for in this analysis.

4.4 Catalogue reliability

The small number of candidate transient sources detected in our search reflects the high reliability of both the GLEAM and TGSS catalogues for point sources with flux densities above $100 - 200$ mJy. The two GLEAM candidates GLEAM J153424−114947 and GLEAM J153653−115052 have been removed from the publicly available GLEAM catalogue. We note that this introduces a small bias in the GLEAM catalogue, since there will be similar artefacts that are weaker than our flux density cutoff that have not been removed.

The importance of rigorous analysis of imaging data to confirm or rule out candidates was demonstrated by Frail et al. (2012) who re-analysed VLA archival data to rule out the long-standing Bower et al. (2007) candidates. Our work provides a good example of this; in an attempt to confirm our transient candidates we reprocessed the relevant data

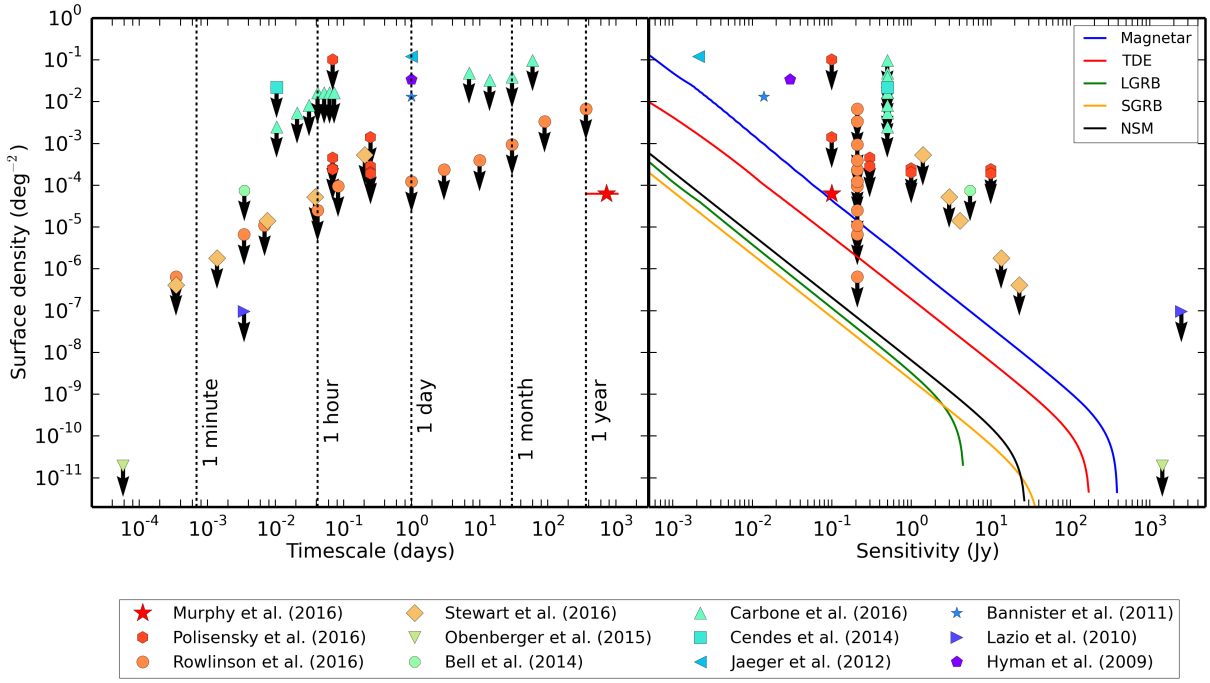

Figure 8. Limits on the transient rates from our survey compared to previously published results at low frequency (< 1 GHz). The result presented in this paper is shown as a red star. The red error bar shows the uncertainty in timescale, as our data spans 1 to 3 years. The coloured lines show the sky density of sources above flux density F_ν for frequency $\nu = 150$ MHz. We have included predicted source rates for various source classes from Figure 3 in Metzger et al. (2015), specifically: magnetars (blue); off-axis tidal disruption events (red); long GRBs with $\theta_{\rm obs} = 1.57$ (green); off-axis short GRBs (orange); and neutron star merger leaving black hole (black). See Metzger et al. (2015) for a detailed description of how these model predictions were calculated.

for both GLEAM and TGSS, and in two cases established that the candidates were imaging artefacts.

5 CONCLUSIONS

We have conducted a blind search for low frequency radio transients by comparing the GLEAM and TGSS ADR1 surveys at 200 and 147.5 MHz respectively. From a total sample of 234 333 GLEAM sources and 275 612 TGSS ADR1 sources in the overlap region between the two surveys, there were 99 658 GLEAM sources and 38 978 TGSS ADR sources that passed our flux density cutoff and compactness criteria. From this sub-sample we found three candidate transient sources, but further analysis identified two of these as imaging artefacts. We present one candidate transient: TGSSADR J183304.4−384046, that has a flux density of 304 mJy at 147.5 MHz (scaled to 182 ± 26 mJy based on a flux scale comparison with GLEAM in the region of the source). This source was not detected in the GLEAM survey 3 years later, implying it had faded to below < 41 mJy. It was also not detected in other archival radio data, or in our ATCA observations.

Based on this detection we calculated a surface density estimate of $\rho = 6.2 \times 10^{-5}$ deg^{-2} for low-frequency radio transients on timescales of 1 to 3 years.

It is worth noting that the distinction between transients and extremely variable sources can be merely a selection effect due to the limited sensitivity and sampling of a given survey. A more comprehensive analysis of variability in this dataset is ongoing. We are also conducting further follow-up observations of TGSSADR J183304.4−384046 in order to classify it.

ACKNOWLEDGMENTS

We thank David McConnell and Richard Hunstead for providing archival radio data from the ATPMN and Molonglo 408 MHz surveys, respectively. We also thank Brian Metzger for providing the model predictions for Figure 8. This research was conducted by the Australian Research Council Centre of Excellence for All-sky Astrophysics (CAASTRO), through project number CE110001020. DLK and SDC are additionally supported by NSF grant AST-1412421. This research work has used the TIFR GMRT Sky Survey (http://tgss.ncra.tifr.res.in) data products. We thank the staff of the GMRT that made these observations possible. GMRT is run by the National Centre for Radio Astrophysics of the Tata Institute of Fundamental Research. The national facility capability for SkyMapper has been funded through ARC LIEF grant LE130100104 from the Australian Research Council, awarded to the University of Sydney, the Australian National University, Swinburne University of Technology, the University of Queensland, the University of Western Australia, the University of Melbourne, Curtin University of Technology, Monash University and the Australian Astronomical Observatory. SkyMapper is owned

and operated by The Australian National University's Research School of Astronomy and Astrophysics.

This scientific work makes use of the Murchison Radioastronomy Observatory, operated by CSIRO. We acknowledge the Wajarri Yamatji people as the traditional owners of the Observatory site. Support for the operation of the MWA is provided by the Australian Government (NCRIS), under a contract to Curtin University administered by Astronomy Australia Limited. We acknowledge the Pawsey Supercomputing Centre which is supported by the Western Australian and Australian Governments.

REFERENCES

Abada-Simon M., Aubier M., 1997, A&AS, 125
Baars J. W. M., Genzel R., Pauliny-Toth I. I. K., Witzel A., 1977, A&A, 61, 99
Bannister K. W., Murphy T., Gaensler B. M., Hunstead R. W., Chatterjee S., 2011, MNRAS, 412, 634
Bell M. E., et al., 2014, MNRAS, 438, 352
Berger E., 2006, ApJ, 648, 629
Bignall H. E., Croft S., Hovatta T., Koay J. Y., Lazio J., Macquart J. P., Reynolds C., 2015, Advancing Astrophysics with the Square Kilometre Array (AASKA14), p. 58
Bower G. C., et al., 2007, ApJ, 666, 346
Bowman J. D., et al., 2013, PASA, 30, 31
Burlon D., Ghirlanda G., van der Horst A., Murphy T., Wijers R. A. M. J., Gaensler B., Ghisellini G., Prandoni I., 2015, Advancing Astrophysics with the Square Kilometre Array (AASKA14), p. 52
Carbone D., et al., 2016, MNRAS, 459, 3161
Castelli F., Kurucz R. L., 2004, in Piskunov N., et al. eds, IAU Symp. No 210, Modelling of Stellar Atmospheres New Grids of ATLAS9 Model Atmospheres
Cendes Y., et al., 2014, arXiv:1412.3986
Clarke T., Kassim N., Polisensky E., Peters W., Giacintucci S., Hyman S. D., 2016, arXiv:1603.03080
Condon J. J., Cotton W. D., Greisen E. W., Yin Q. F., Perley R. A., Taylor G. B., Broderick J. J., 1998, AJ, 115, 1693
Cordes J. M., et al., 2004, New Astronomy Reviews, 48, 1459
Cordes J. M., Lazio T. J. W., 2002, arXiv:0207156
Covey K. R., Ivezić Ž., Schlegel D., Finkbeiner D., Padmanabhan N., Lupton R. H., Agüeros M. A., Bochanski J. J., Hawley S. L., West A. A., Seth A., Kimball A., Gogarten S. M., Claire M., Haggard D., Kaib N., Schneider D. P., Sesar B., 2007, AJ, 134, 2398
Croft S., Bower G. C., Whysong D., 2013, ApJ, 762, 93
Drimmel R., Cabrera-Lavers A., López-Corredoira M., 2003, A&A, 409, 205
Fender R., 2006, Jets from X-ray binaries. pp 381–419
Fender R., Stewart A., Macquart J.-P., Donnarumma I., Murphy T., Deller A., Paragi Z., Chatterjee S., 2015, arXiv:1507.00729
Fiedler R. L., et al., 1987, Nature, 326, 675
Frail D. A., Kulkarni S. R., Ofek E. O., Bower G. C., Nakar E., 2012, ApJ, 747, 70
Fujii Y., Spiegel D. S., Mroczkowski T., Nordhaus J., Zimmerman N. T., Parsons A. R., Mirbabayi M., Madhusudhan N., 2016, ApJ, 820, 122
Grießmeier J.-M., Zarka P., Girard J. N., 2011, Radio Science, 46, 0
Gürkan G., Hardcastle M. J., Jarvis M. J., 2014, MNRAS, 438, 1149
Hancock P., Gaensler B. M., Murphy T., 2011, ApJ, 735, L35
Hawley S. L., et al., 2002, AJ, 123, 3409
Hess S. L. G., Zarka P., 2011, A&A, 531, A29
Hughes P. A., Aller H. D., Aller M. F., 1992, ApJ, 396, 469
Hurley-Walker N., et al., 2016, Submitted
Hyman S. D., et al., 2005, Nat, 434, 50
Hyman S. D., Wijnands R., Lazio T. J. W., Pal S., Starling R., Kassim N. E., Ray P. S., 2009, ApJ, 696, 280
Intema H. T., et al., 2009, A&A, 501, 1185
Intema H. T., Jagannathan P., Mooley K. P., Frail D. A., 2016, arXiv:1603.04368
Jaeger T. R., Hyman S. D., Kassim N. E., Lazio T. J. W., 2012, AJ, 143, 96
Jaeger T. R., Osten R. A., Lazio T. J., Kassim N., Mutel R. L., 2011, AJ, 142, 189
Kaplan D. L., et al., 2015, ApJ, 809, L12
Keane E. F., et al., 2016, Nat, 530, 453
Keller S. C., et al., 2007, PASA, 24, 1
Lane W. M., Cotton W. D., van Velzen S., Clarke T. E., Kassim N. E., Helmboldt J. F., Lazio T. J. W., Cohen A. S., 2014, MNRAS, 440, 327
Lazio T. J. W., Shankland P. D., Farrell W. M., Blank D. L., 2010, AJ, 140, 1929
Loi S. T., et al., 2015, MNRAS, 453, 2731
Mauch T., Murphy T., Buttery H. J., Curran J., Hunstead R. W., Piestrzynski B., Robertson J. G., Sadler E. M., 2003, MNRAS, 342, 1117
McConnell D., Sadler E. M., Murphy T., Ekers R. D., 2012, MNRAS, 422, 1527
Metzger B. D., Williams P. K. G., Berger E., 2015, ApJ, 806, 224
Murphy T., et al., 2015, MNRAS, 446, 2560
Nelson G. J., Robinson R. D., Slee O. B., Fielding G., Page A. A., Walker W. S. G., 1979, MNRAS, 187, 405
Obenberger K. S., et al., 2015, Journal of Astronomical Instrumentation, 4, 1550004
Polisensky E., Lane W. M., Hyman S. D., Kassim N. E., Giacintucci S., Clarke T. E., Cotton W. D., Cleland E., Frail D. A., 2016, arXiv:1604.00667
Polletta M., et al., 2007, ApJ, 663, 81
Readhead A. C. S., 1994, ApJ, 426, 51
Rowlinson A., et al., 2016, MNRAS, 458, 3506
Scaife A. M. M., Heald G. H., 2012, MNRAS, 423, L30
Skrutskie M. F., et al., 2006, AJ, 131, 1163
Sobey C., et al., 2015, MNRAS, 451, 2493
Spangler S. R., Moffett T. J., 1976, ApJ, 203, 497
Stern D., Assef R. J., Benford D. J., Blain A., Cutri R., Dey A., Eisenhardt P., Griffith R. L., Jarrett T. H., Lake S., Masci F., Petty S., Stanford S. A., Tsai C.-W., Wright E. L., Yan L., Harrison F., Madsen K., 2012, ApJ, 753, 30
Stewart A. J., et al., 2016, MNRAS, 456, 2321
Swarup G., 1990, Indian Journal of Radio and Space Physics, 19, 493

Taylor G. B., et al., 2012, Journal of Astronomical Instrumentation, 1, 1250004
Tingay S. J., et al., 2013, PASA, 30, 7
van Haarlem M. P., et al., 2013, A&A, 556, A2
van Weeren R. J., et al., 2016, ApJS, 223, 2
Vardoulaki E., Rawlings S., Hill G. J., Mauch T., Inskip K. J., Riley J., Brand K., Croft S., Willott C. J., 2010, MNRAS, 401, 1709
Wayth R. B., et al., 2015, PASA, 32, 25
Williams P. K. G., Berger E., 2016, ApJ, 821, L22
Willott C. J., Rawlings S., Jarvis M. J., Blundell K. M., 2003, MNRAS, 339, 173
Wright E. L., et al., 2010, AJ, 140, 1868
Zarka P., Treumann R. A., Ryabov B. P., Ryabov V. B., 2001, Astrophys. Space. Sci., 277, 293